Journal of Neuroscience Methods 286 (2017) 38–55

Contents lists available at ScienceDirect

Journal of Neuroscience Methods

journal homepage: www.elsevier.com/locate/jneumeth

3D printing and modelling of customized implants and surgical guides for non-human primates

Xing Chen[a,*], Jessy K. Possel[a], Catherine Wacongne[a], Anne F. van Ham[a], P. Christiaan Klink[a,b,c,d], Pieter R. Roelfsema[a,c,d]

[a] Department of Vision & Cognition, Netherlands Institute for Neuroscience, Meibergdreef 47, 1105 BA, Amsterdam, Netherlands
[b] Department of Neuromodulation & Behaviour, Netherlands Institute for Neuroscience, Meibergdreef 47, 1105 BA, Amsterdam, Netherlands
[c] Department of Integrative Neurophysiology, VU University, De Boelelaan 1085, 1081 HV, Amsterdam, Netherlands
[d] Department of Psychiatry, Academic Medical Center, Postbus 22660, 1100 DD, Amsterdam, Netherlands

HIGHLIGHTS

- We created affordable, customized, 3D-printed cranial implants for electrophysiology.
- These included head posts, recording chambers, and pedestal base plates.
- Scale models and craniotomy guides were also used during planning and surgery.
- Animal welfare was enhanced during surgery and risk of infection reduced.
- To date, our implants remain robust and well-integrated with the skull.

GRAPHICAL ABSTRACT

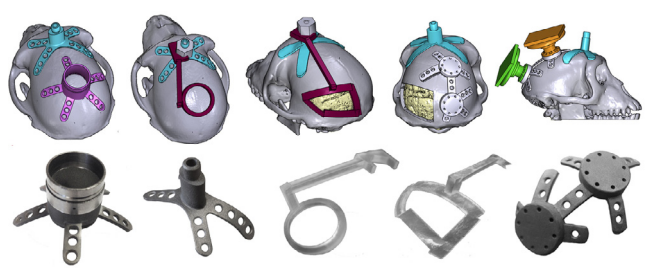

ARTICLE INFO

Article history:
Received 9 March 2017
Received in revised form 5 May 2017
Accepted 8 May 2017
Available online 13 May 2017

Keywords:
3D printing
Cranial implants
Electrophysiology
Primate

ABSTRACT

Background: Primate neurobiologists use chronically implanted devices such as pedestals for head stabilization and chambers to gain access to the brain and study its activity. Such implants are skull-mounted, and made from a hard, durable material, such as titanium.

New method: Here, we present a low-cost method of creating customized 3D-printed cranial implants that are tailored to the anatomy of individual animals. We performed pre-surgical computed tomography (CT) and magnetic resonance (MR) scans to generate three-dimensional (3D) models of the skull and brain. We then used 3D modelling software to design implantable head posts, chambers, and a pedestal anchorage base, as well as craniotomy guides to aid us during surgery. Prototypes were made from plastic or resin, while implants were 3D-printed in titanium. The implants underwent post-processing and received a coating of osteocompatible material to promote bone integration.

Results: Their tailored fit greatly facilitated surgical implantation, and eliminated the gap between the implant and the bone. To date, our implants remain robust and well-integrated with the skull.

Comparison with existing method(s): Commercial-off-the-shelf solutions typically come with a uniform, flat base, preventing them from sitting flush against the curved surface of the skull. This leaves gaps for fluid and tissue ingress, increasing the risk of microbial infection and tissue inflammation, as well as implant loss.

Conclusions: The use of 3D printing technology enabled us to quickly and affordably create unique, complex designs, avoiding the constraints levied by traditional production methods, thereby boosting experimental success and improving the wellbeing of the animals.

© 2017 The Author(s). Published by Elsevier B.V. This is an open access article under the CC BY-NC-ND license (http://creativecommons.org/licenses/by-nc-nd/4.0/).

* Corresponding author at: Netherlands Institute for Neuroscience, Meibergdreef 47, 1105 BA, Amsterdam, Netherlands.
E-mail address: x.chen@nin.knaw.nl (X. Chen).

http://dx.doi.org/10.1016/j.jneumeth.2017.05.013
0165-0270/© 2017 The Author(s). Published by Elsevier B.V. This is an open access article under the CC BY-NC-ND license (http://creativecommons.org/licenses/by-nc-nd/4.0/).

1. Introduction

Primate electrophysiologists use a range of implantable devices to access and record from brain regions of interest. For electrode recordings in awake animals, the subjects are often implanted with recording chambers, which protect the brain from the external environment in between experiments (Evarts, 1966; Gardiner and Toth, 1999; Adams et al., 2011). During recordings, researchers can open up the chamber and insert electrodes directly into the brain, sampling neuronal activity at various depths and spatial locations. For chronic multicellular recordings, researchers may choose to implant electrode arrays containing dozens of recording sites into the brain. These arrays are connected to a skull-mounted pedestal via transcranial wires (Campbell et al., 1991; Nordhausen et al., 1994; Nicolelis et al., 2003). An interface consisting of either electrical contact points or a wireless transceiver unit is mounted on the pedestal, providing a connection to external equipment. Furthermore, when performing acute recordings, or when a task necessitates the spatial stabilization of images on the retina, fixation of the head is commonly achieved using a single-piece, screw-mounted head post (Adams et al., 2007), or an equivalent device with multiple contact points on the skull (Pigarev et al., 1997; Isoda et al., 2005).

For each of these applications, the implant must remain firmly fixed to the skull over extended periods of time. Poorly fitting implants may fail to integrate with the bone, come loose, or break off, affecting the welfare of the animals and disrupting experiments (Johnston et al., 2016). Here, we describe how new 3D printing techniques can be used to ensure a seamless fit between the bone and the implant, and to facilitate surgical implantation. We also describe the use of 3D modelling during pre-surgical planning to enhance the accuracy of electrode insertion.

The technique of 3D printing refers to the process of using a machine to additively assemble a 3D object layer by layer, using a digital design as a blueprint. This approach allows for highly customizable designs, which can be printed in small quantities at affordable prices, due to the relatively low set up costs and minimal wastage of material. Manufacturers can choose from a growing range of materials, including plastics, metals, ceramics, and wood, with various degrees of hardness, strength, durability, and elasticity. These methods are hence gaining popularity for use in the laboratory. Recent applications of 3D printing in neuroscience include 3D-printed models of neuronal cell types for visualization of their morphology (McDougal and Shepherd, 2015), as well as 3D-printed lab equipment, such as micromanipulators (Patel et al., 2014; Baden et al., 2015) and cortical recording platforms, cranial windows, and perfusion chambers for rodent experiments (Tek et al., 2008). To promote the sharing of scientific 3D models, the National Institutes of Health recently launched the NIH 3D Print Exchange- a free and publicly accessible online repository for 3D-printable models in the fields of biology and medicine (https://3dprint.nih.gov/). Here, we focus on the use of 3D printing for the creation of customized cranial implants in non-human primate (NHP) neurophysiology experiments.

Typically, implants used in NHP neurobiology, such as head posts and chambers, are one-size-fits-all solutions that can be purchased from companies such as Crist Instrument Co., Inc (for a few hundred euros). These off-the-shelf implants require time-consuming manual adjustments during each surgical procedure (Adams et al., 2007, 2011; Mulliken et al., 2015), such as bending of the legs of the implant with pliers or tapping them with a hammer. However, even if the legs are pliable, a portion of the base is sometimes flat and rigid (as seen, for example, in Fig. 1A, or the head post designed by Adams et al., 2007), making it impossible to obtain a curved surface. Even after bending of the legs, the fit between the implant and the skull is often imperfect, making it harder for the implant to integrate with the bone. Furthermore, the space between the metal and the bone increases the risk of unwanted growth of granulation tissue in the gap between the skull and the implant, which may contribute to infection and inflammation, bone and skin degradation, implant instability, and even implant failure (Galashan et al., 2011; Johnston et al., 2016; Raphel et al., 2016).

If a study involves functional imaging experiments, then metal implants typically cannot be used as they interfere with the magnetic field in the scanner and generate an artefact in the signal. Instead, the implants are generally made from radiolucent material such as polyether ether ketone (PEEK) or polyetherimide (PEI). As the technology for 3D printing with these MR-compatible materials is still at an early stage of development, we here focus on 3D printing in titanium. However, it is conceivable that 3D printing with MR-compatible materials will be possible in the future.

For electrophysiology that involves chronically recording from dozens of neurons, the CerePort™ from Blackrock Microsystems (Salt Lake City, Utah) is a popular tool in many primate neuroscience labs. Its FDA-approved, CE-marked counterpart, the NeuroPort™, is used in clinical trials with human patients (Collinger et al., 2013; Flesher et al., 2016). The CerePort™ pedestal provides a percutaneous interface between the implanted multielectrode arrays and the external data acquisition equipment (Fig. 1B), via an electronic interface board (EIB) that is screwed onto the upper half of the pedestal during each experimental session. The base of the pedestal contains eight screw holes, allowing it to be mounted on the skull. However, the diameter of the pedestal base is small and it lacks legs, concentrating the screws over a limited surface area. Furthermore, the base of the pedestal is flat and does not sit flush against the skull, which may contribute to problems with infection and implant detachment. One possible solution is to improve the attachment to the bone using dental cement. However, in some animals, tissue builds up between the bone and the cement with time, thus creating a space that is susceptible to microbial infection. Another possible solution is to shave the bone down, in order to create a flat surface. However, it is not easy to remove sufficient bone so that the flat surface of the implant fits well, and in addition, this technique reduces the thickness of the skull underneath the implant, which may create a weak spot. Hence, we sought to create implants that provide a better fit with the skull than these commercial-off-the-shelf solutions.

In previous studies, customized implants were designed using anatomical scans of the individual animal's skull, ensuring a good fit between the bone and the implant, reducing the duration of surgery, and decreasing the likelihood of granulation tissue growth and infection (McAndrew et al., 2012; Lanz et al., 2013). These implants were typically manufactured using computer numerical control (CNC) machines, which use traditional milling methods to 'sculpt' objects out of a solid block of starting material, under the control of computer-aided design (CAD) programmes. Several research labs carry out their design process and production using CAD software and CNC machines, either in-house (Galashan et al., 2011; Lanz et al., 2013; Mulliken et al., 2015) or outsourced to a CNC workshop (Adams et al., 2007) or a company that specializes in such implants (Johnston et al., 2016). Several companies offer CNC milling services to create customized solutions for a small range of implantable products (e.g. Crist Instruments Co., Inc, Hagerstown, MD; Gray Matter Research, Bozeman, MT; Rogue Research Inc., Montreal, Canada).

A drawback of these techniques is that they are costly, for several reasons: CNC machines still rely on traditional techniques, such as drilling and sawing, to generate the final product. The use of CNC milling thus requires substantial expertise and training, with an understanding of the constraints imposed by the tooling-path limitations of the milling devices. To reduce the weight of an implant,

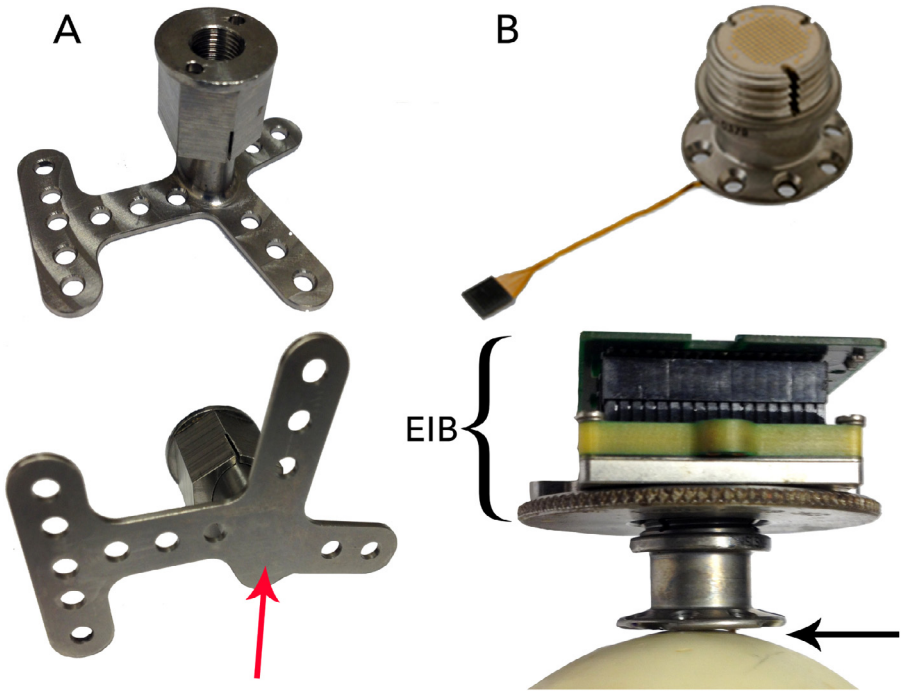

Fig. 1. A) One-size-fits-all head posts, such as the one pictured here, have legs that can be bent into the desired shape. However, the metal at the middle of the base (indicated by the arrow) is relatively thick, and cannot be bent. B) The CerePort^{TM} device consists of one or more electrode arrays that are implanted in the brain, which connect to a skull-mounted pedestal interface via a wire bundle (top). An electronic interface board connects the pedestal to the data acquisition and/or stimulation equipment during each recording session (bottom). The base of the pedestal is flat, leaving a gap between the base and the skull (indicated by the arrow), or requiring thinning of the bone.

for example, it is possible to create internal cavities through CNC milling. However, this leaves spaces for fluid or tissue ingress, increasing the risk of infection. When creating an object with complex and curved geometry, such as a cranial implant, one typically requires a '5-axis' milling machine, which is capable of simultaneously moving a tool along five different axes. Such machines are expensive (with a current market price of M€ 0.5–1). Due to the high setup costs for each design, manufacturers are often compelled to produce these implants in bulk, to ensure that production remains cost-effective. Correspondingly, one-off creations tend to be more expensive. For example, for a customized recording chamber, the companies that we contacted charged between € 1500 and € 3000.

The use of 3D printing methods offers several advantages over CNC-based production methods: (1) Complex structures such as internal cavities, textured surfaces, and intricate shapes can easily be created through 3D printing, allowing for innovative and lightweight designs. The creation of fully enclosed internal cavities within a single, solid object also avoids problems with fluid and tissue ingress and infection. (2) Less material is used, leading to reduced wastage and cost. (3) Setup costs and times are relatively low, while production costs and times are comparable to those of CNC milling. Hence, both prototypes and final versions of implants can be produced rapidly, within a timescale of hours to weeks. (4) Should modifications be required, it is relatively easy to go through multiple iterations of the design, to achieve an ideal solution.

For these reasons, 3D printing is increasingly popular in the clinical realm for the creation of customized medical implants, particularly in orthopaedics, cranio-maxillofacial surgery, and cochlear implant surgery, ensuring a tailored fit to the anatomy of individual patients (Rengier et al., 2010; Parthasarathy, 2014; Chae et al., 2015; Mok et al., 2016). It is also used as an educational and training tool, providing medical personnel and patients with an intuitive understanding of human anatomy, and allowing surgeons to practice their technique on biologically realistic 3D-printed tissues during mock surgeries (Rose et al., 2015a,b). 3D printing has also catalyzed promising developments in the field of tissue engineering, resulting in the creation of biomimetic 3D-printed scaffolds for tissue and organ regeneration (Murphy and Atala, 2014; Chia, 2015; Wu and Hsu, 2015). In medical and commercial settings, clinicians and engineers typically use specialized software packages such as the Mimics Innovation Suite (Materialise, Leuven, Belgium) to design their prosthetic implants. However, subscription costs are often high, amounting to thousands of euros per year.

The benefits of bringing 3D modelling technologies into the field of primate neurobiology have previously been highlighted by McAndrew et al. (2012) and Lanz et al. (2013). McAndrew et al. designed their customized recording chambers using costly software packages (Mimics and SolidWorks), and in both studies, the chambers were then manufactured from radiolucent PEEK material, using CNC milling techniques. The high costs of using the software, as well as unfamiliarity with CNC machining techniques, might constitute a barrier to access and to wide adoption of these new technologies by the research community.

Here, we describe how researchers can make use of free, open-source software to design customized implants, and exploit recent advances in 3D printing to produce affordable, form-fitting metal implants, while eliminating the need for CNC milling (Avila et al., 2012). We will outline the steps involved in the design of head posts, chambers and pedestal anchorage plates that have closely fitting legs and bases, making implantation quick and easy, while leaving little to no room between the bone and the implant. We will also illustrate the mapping of brain vasculature in regions of interest, with the goal of minimizing the damage caused by insertion of electrodes. Finally, we will show how non-invasive anatomical mapping techniques can be used to plan the exact locations of craniotomies and sites of electrode insertion prior to surgery, and describe how to construct guides to mark the desired positions of implants and craniotomies during surgery.

2. Materials and methods

We produced customized implants for male rhesus macaque monkeys, ranging from 4 to 7 years of age and 6.5 to 11.0 kg in weight at the time of implantation. Seven of these animals were implanted with head posts, and two of the seven also received a recording chamber. In one animal, we implanted an anchorage plate that acted as a base for two CerePort™ connectors (Blackrock Microsystems).

In the following sections, we first describe our methods for generating 3D models of the brain and skull, which are crucial for implant design and surgical planning. Next, we describe how we created the customized implants (head posts, chambers, and pedestal anchorage plates), as well as craniotomy guides that were used as aids during surgery.

We made anatomical scans using computed tomography (CT) and magnetic resonance imaging (MRI). CT scans are relatively quick and easy to carry out, and yield excellent images of hard tissue such as bone, hence they were used to generate 3D models of the skull. However, the image quality from a CT scan is not sufficient for clear visualization and segmentation of soft tissue such as the brain. We therefore used structural MRI scans to generate 3D models of the brain. It is possible, but not necessary, to place the animal in a stereotactic frame for these scans. Here, we acquired the CT and MRI scans without using a stereotactic frame.

2.1. Generating a 3D model of the skull

The CT scans were acquired in a Philips Brilliance scanner, with a field of view of ±250 mm, a matrix size of 512, a slice thickness of 0.9 mm, an increment of 0.45 mm, a tube of 120 kV and tube current of 285 mAs, and a rotation time of 0.75 s. For induction of anaesthesia, we administered medetomidine (0.08 ml/kg i.m.) and ketamine (0.07 ml/kg i.m.). If the procedure lasted for over 30 minutes, a second dose of ketamine (0.07 ml/kg) was given. When returning the monkey to its home cage, we administered an antagonist, atipamezole (0.08 ml/kg i.m.).

We imported 'digital imaging and communications in medicine' (DICOM) images from the CT scans into either InVesalius 3.0 (Windows) or OsiriX Lite 7.5.1 (Mac). Using this free software, we performed automatic thresholding and segmentation to generate a 3D model of the skull (Fig. 2). The model was exported in the STereoLithography (STL) format, which describes the surface geometry of a three-dimensional object using a triangulated Cartesian coordinate system, and is compatible with many 3D modelling software packages. STL is the industry standard in 3D printing, and it does not intrinsically specify the model units (e.g. mm, cm, inches). Our modelling was always carried out using units of millimetres, and we did not encounter any difficulties when exporting STL files or sharing them between various software programmes. For a more detailed description of how this was carried out, please refer to the document titled, 'How to create a 3D mesh STL from DICOM' in the Supplementary Information.

2.2. Generating a 3D model of the brain

To aid the planning and design of our customized implants, we carried out anatomical MRI scans and generated 3D models of the brain to identify regions of interest. This non-invasive approach allowed us to optimize the location of each implant, and tailor it to the anatomy of individual animals. For animals that received multiple implants, such as a head post and a recording chamber or a head post and a pedestal anchorage base, we verified that the implants were spaced sufficiently far apart from each other. Where possible, we conducted our MRI scans before implanting the animals with a titanium head post, to ensure that the MRI images would be free of metal-induced artefacts.

The MRI scans were acquired in a Philips Ingenia CX 3T scanner, with a 3D T1-TFE gradient echo pulse sequence, SAG SENSE parallel imaging, a matrix size of 512, a slice thickness of 0.5 mm, an increment of 0.5 mm, sequential acquisition of slices, and TE = 7.3 ms, TR = 15.9 ms, and flip angle of 8°. The anaesthesia protocol was identical to that of the CT scans, as described in Section 2.1.

Segmentation of the brain could be performed in either one of two ways: largely automatically on a Linux operating system, or semi-automatically on a Windows or Mac platform. For automatic segmentation of the whole brain (Linux), we converted the DICOM images that were generated from the MRI scans into compressed NIfTI files using either the dcm2nii or dcm2niix tool (Li et al., 2016, https://www.nitrc.org/projects/dcm2nii/) and processed them in FSL 5.0.9 (FMRIB, Oxford, UK, https://fsl.fmrib.ox.ac.uk/fsl/fslwiki/FSL). The Brain Extraction tool (BET) v2.1 was used for skull stripping, to generate the isolated brain volume. Next, the FAST automatic segmentation tool was used to differentiate between cerebral spinal fluid, white matter and grey matter, generating output volumes for these three types of tissue. The segmented volume was then imported into 3D Slicer 4.4.0, where the tissue types were converted into 3D models using the Model Maker function, and exported in STL format (Fig. 3). For a more detailed description of how this was carried out, please refer to the document titled, 'Automatic brain segmentation' in the Supplementary Information.

For segmentation of individual brain regions (e.g. the superior colliculus and visual cortex), or for segmentation of the whole brain on non-Linux operating systems, we imported the DICOM images from the MRI scans directly into 3D Slicer. We identified regions of interest with the aid of a stereotaxic atlas (The Rhesus Monkey Brain in Stereotaxic Coordinates, Paxinos et al., 1999), and we performed slice-by-slice semi-automatic segmentation of the brain or region of interest using the Editor module (Fig. 4). For a more detailed description of how this was carried out, please refer to the document titled, 'Slicer manual' in the Supplementary Information. We then generated models of brain tissue and exported them as STL files.

2.3. Generating a 3D model of blood vasculature

The brain is supplied by a vast network of vessels, with some of the large vessels located on the surface of the brain, and cortical arteries and veins running perpendicular to the surface (Weber et al., 2008). For studies in which large numbers of electrodes are inserted into the cortex (for example, using Utah arrays from Blackrock Microsystems), we hypothesized that it would be useful to non-invasively obtain anatomical models of the brain vasculature, prior to surgical insertion of the arrays. This would aid the planning of the layout of arrays upon the cortical surface, and avoid damaging large blood vessels. We tested the feasibility of this approach in one animal.

In this animal, a contrast-enhanced MR angiography (CE-MRA) was performed during an MRI scan session, to identify the anatomical location of blood vessels. This was carried out in a Philips Ingenia CX 3T scanner, with a T1-FFE gradient echo pulse sequence, window width = 795 HU, window level = 408 HU, a matrix size of 336, a slice thickness of 1 mm, an increment of 0.5 mm, a coronal acquisition orientation, sequential acquisition of slices, TE = 1.9 ms, TR = 4.0 ms, and flip angle of 18°. The animal was anaesthetized (as described in Section 2.1) and head-fixed in a stereotaxic frame to ensure stability of the image. A gadolinium tracer (0.15 ml/kg), also known as contrast dye, was intravenously infused, followed by an infusion of 0.9% NaCl to flush out the contrast dye. Two sequences were obtained: one prior to infusion of gadolinium, and the other

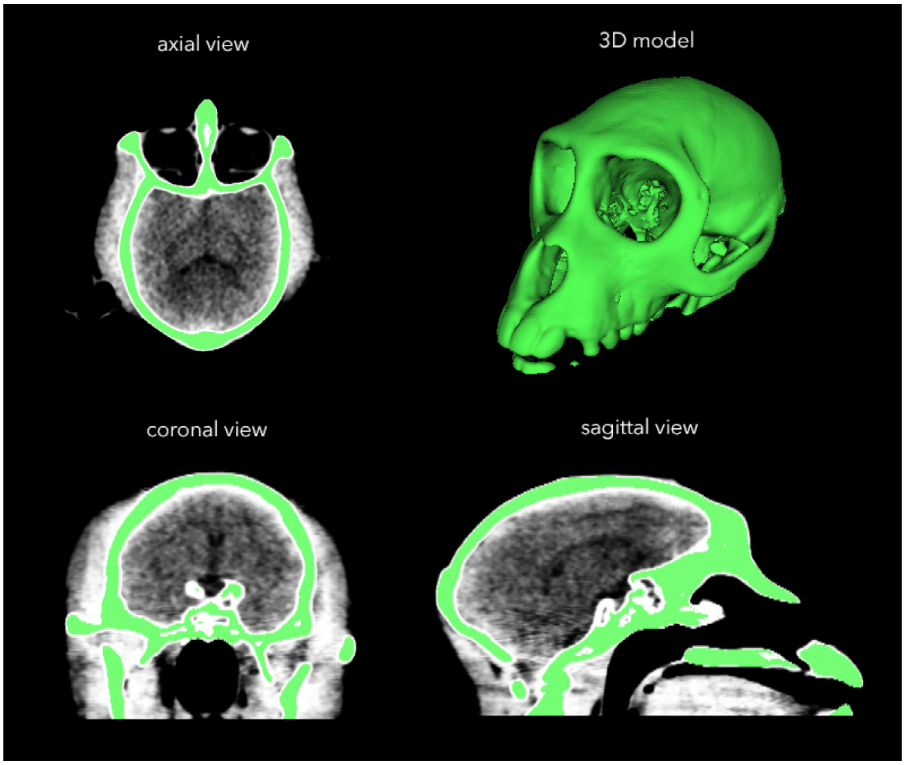

Fig. 2. After carrying out a CT scan, we used InVesalius software to generate a 3D model of the skull from DICOM files.

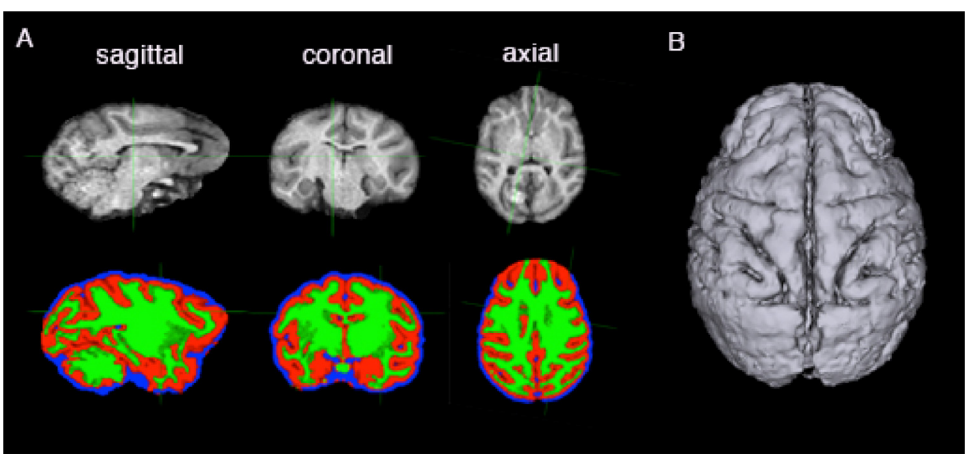

Fig. 3. We performed automatic extraction and tissue segmentation of the whole brain from MRI data using FSL software (A), and converted the segmented volumes into surfaces using 3D Slicer (B).

during the infusion of gadolinium. Using the MR scanner software, the sequence that was obtained in the first series was subtracted from that obtained in the second, and a maximum intensity projection (MIP) of the subtraction data was generated, allowing the visualization of blood vessels of ≥0.4 mm in diameter.

We imported the MRA subtraction images (in DICOM format) into InVesalius, and used the software to segment the images via automated threshold setting. We generated a 3D model of the vasculature, which we then exported in STL format.

2.4. Alignment of models

We imported the STL models of the skull, brain tissue, and blood vessels into MeshLab 1.3.4 beta, and removed loose fragments using the Cleaning and Repairing tool, 'Remove isolated pieces with regard to diameter.' The Laplacian smoothing function was used to smooth the surfaces of the models.

We exported the cleaned and smoothed models as STL files, and imported them into 3D Slicer. The models of the skull, brain, and blood vessels were manually aligned using the Transformation module in 3D Slicer (Figs. 5 and 6). We then exported the transformed models as STL files for further processing.

2.5. 3D modelling of implants

Software that is used for 3D modelling and design can be broadly categorized into two groups: some are optimized for the design of top-down, precisely engineered objects (e.g. tools and mechanical parts), while others are better suited for the creation and handling

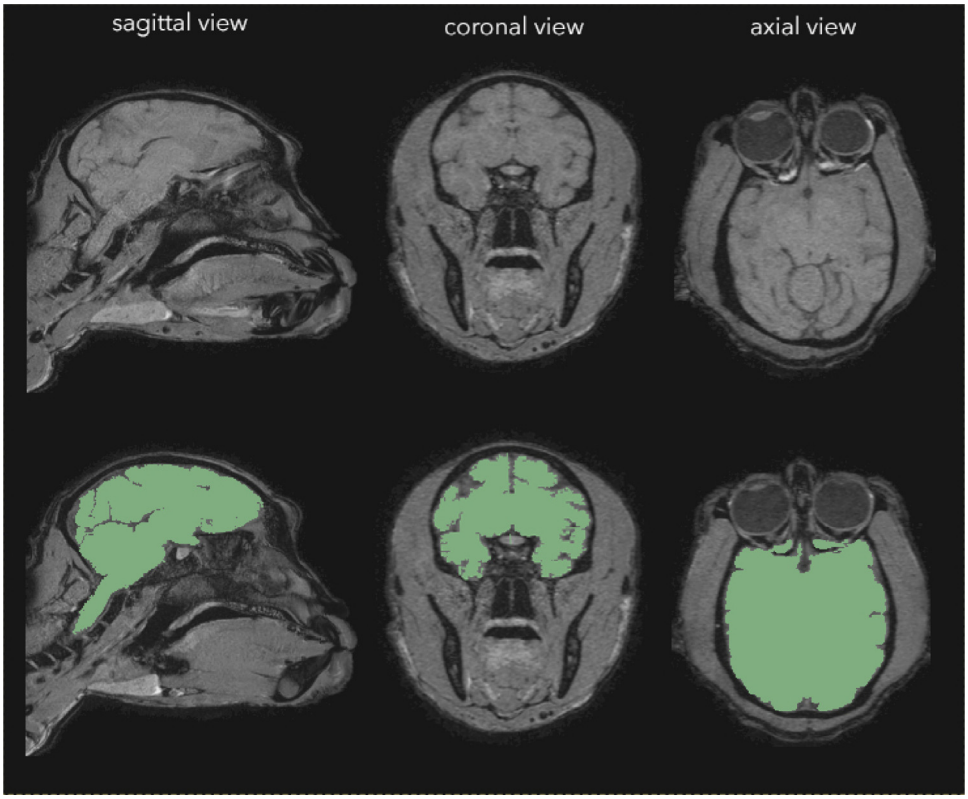

Fig. 4. We performed manual segmentation of the brain (green regions) on MRI data using 3D Slicer software (colours are visible in the online version of the paper).

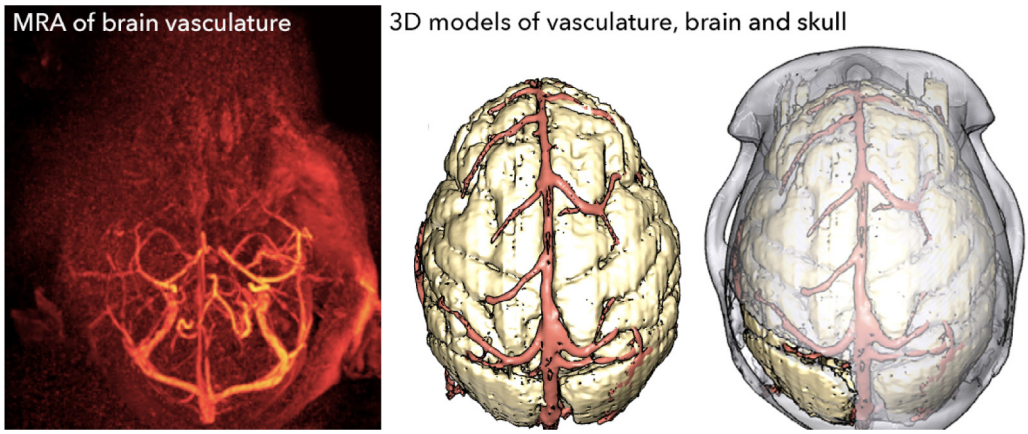

Fig. 5. We performed an MRA in one animal, and visualized the blood vessels InVesalius software (left). We generated a 3D model of the blood vessels, and aligned it with 3D models of the brain and skull using 3D Slicer.

of complex, naturalistic-looking objects (e.g. animals and plants). A few are capable of handling both types of data.

For the in-house creation of most of our customized objects (head posts, craniotomy guides, and pedestal anchorage bases), we used a combination of Autodesk Inventor Professional 2015 and Blender 2.76 software. Blender is a free, open-source 3D engineering and design software that is suitable for the modelling of mechanically engineered parts, while being powerful and agile enough to handle complex biological data. Hence, it had the advantage of being able to perform all the modelling functions that we needed, while being freely available. For the modelling of parts with simple geometry, we also used Inventor, a proprietary software that is popular for 3D mechanical design. However, we found it to be less suitable for working with biological data, as attempts to import a model of a complex structure such as the skull would cause the software to crash when running on an Intel® Core ™ i7-4771 HP computer with 32 GB of usable RAM. Other software packages, such as SolidWorks (Dassault Systemes) and 3-matic (Materialise), are proprietary software that accomplish similar tasks to Blender, and our recording chambers were designed by an external contractor using SolidWorks. We note, however, that these models could also have been made free-of-charge using Blender. For more detailed instructions on how to use Blender for modelling of customized objects, please refer to the document titled, 'Blender manual' in the Supplementary Information.

For each of the 3D-designed objects, we identified key anatomical landmarks, such as the locations of targeted brain regions and the occipital ridge (indicated by the arrow in Fig. 6). We used these to plan the precise position and design of implants, optimize the site of craniotomies, and ensure that in the case of animals with

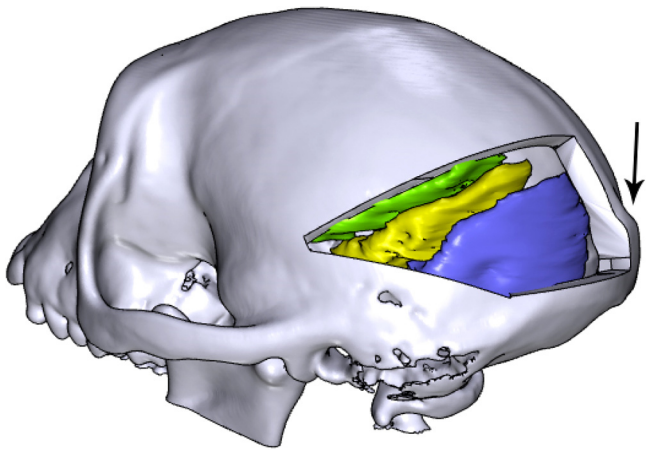

Fig. 6. Different regions of the visual cortex, such as V1 and V2 (purple), V3 and V4 (yellow), and other areas (green) were coarsely segmented and aligned with the skull using 3D Slicer (colours are visible in the online version of the paper). We used anatomical landmarks, such as the occipital ridge (indicated by the arrow), to identify the sites of craniotomies and implants.

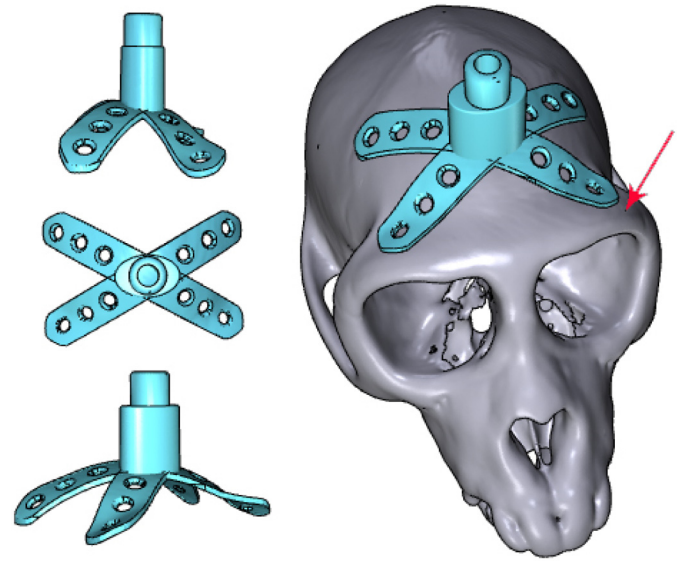

Fig. 7. Head posts with customized bases and legs were modelled using a combination of Inventor and Blender software. The anteriormost parts of the head posts were positioned several milimetres away from the supraorbital ridge (indicated by the arrow).

multiple implants (e.g. a head post and a recording chamber), the implants were spaced apart from each other. In some cases, particularly when planning the site of craniotomies for electrophysiology, the region of interest was identifiable primarily through stereotaxic coordinates, rather than anatomical landmarks. When we designed our recording chambers, for example, we used stereotaxic coordinates to determine the precise location of the chamber on the skull (more details are provided in Section 2.7). Certain features could not be 3D printed (e.g. screw threads, narrow pins, grooves, and small holes), and hence required manual machining. Our mechanical engineers advised us on the design of these features. For example, we ordered taps and dies to create screw threads of the desired sizes on the head posts and pedestal anchorage base, and ensured that the design of the prints allowed them to be clamped securely during the addition of screw threads.

2.6. Modelling of head posts for head fixation

The design of the top portion of the head post was standardized across animals, to ensure compatibility with lab equipment. We created this part in Inventor, and subsequently imported it into Blender in the STL format. The design called for a screw thread at the top of the head post, which was too fine to be 3D-printed. Hence, we printed this element as a solid rod, and the screw thread was added manually after 3D printing. We modelled the base and legs of the head post using Blender, and tailored them to the curvature of the animal's skull (Fig. 7). When planning the location of our customized head posts, we ensured that the front legs of the head posts were positioned close to but not less than ~2 mm from the anterior-most part of the supraorbital ridge (also known as the eyebrow bone). For a more detailed description of how this was carried out, please refer to the document titled, 'How to create a custom-designed head post' and the template file, 'template_head_post.blend' in the Supplementary Information.

2.7. Modelling of recording chambers

For our superior colliculus (SC) experiments, we planned the position of the recording chambers using the external ear canals as stereotaxic landmarks to obtain the location of AP0, and identified the horizontal plane that passed through the interaural line and the infraorbital ridge. We used a stereotaxic atlas (Paxinos et al., 1999) to locate the SC, and segmented the structure using 3D Slicer. We generated three perpendicular model planes, and positioned them such that one plane passed through the interaural line and the infraorbital ridge, another passed through the midsagittal plane, and the last passed through the SC (Fig. 8). STL files containing models of the skull, SC, and planes were sent to an external contractor, who designed the chamber using SolidWorks software. To ensure that the SC would be accessible to electrodes that were inserted through the chamber, the chamber was oriented to match the trajectory of electrodes, and centred on the point of intersection between the skull and the two planes that ran through the SC. The legs and base of the chamber were custom-fit to the curvature of the skull.

2.8. Modelling of pedestal anchorage bases

In one of the monkeys, we aimed to chronically implant Utah arrays into the right hemisphere of the visual cortex, and two standard CerePort™ pedestals (Blackrock Microsystems) on the skull over the left hemisphere. This necessitated careful planning of the locations of electrode arrays on the visual cortex, and calculation of the location and size of the corresponding craniotomy. We first carried out a segmentation of the whole brain, as described above, and identified the location of V1 and V4 using anatomical landmarks such as the lunate sulcus. We then determined the boundaries of the craniotomy that would be made during surgery. This allowed us to choose the precise location of our implant(s) on the skull, ensuring that they did not overlap with the craniotomy or with the head post (Fig. 9).

CerePort™ pedestals have a flat base that is not tailored to the curvature of the animal's skull (Fig. 1B), and they sometimes detach from the bone. Hence, we designed a customized pedestal anchorage base that acted as an interface for the two pedestals (Fig. 9) while ensuring a close fit to the skull. The upper surfaces of the pedestal anchorage base were designed in Inventor, and included screw holes for the subsequent attachment of the two CerePort™ pedestals. The screw threads themselves were too fine to be 3D printed. We therefore added holes as markers, to which screw threads would later be added. Models of the CerePort™ pedestals and their USB mating interface were also created using Inventor, and all the models were imported into Blender. The CerePort™

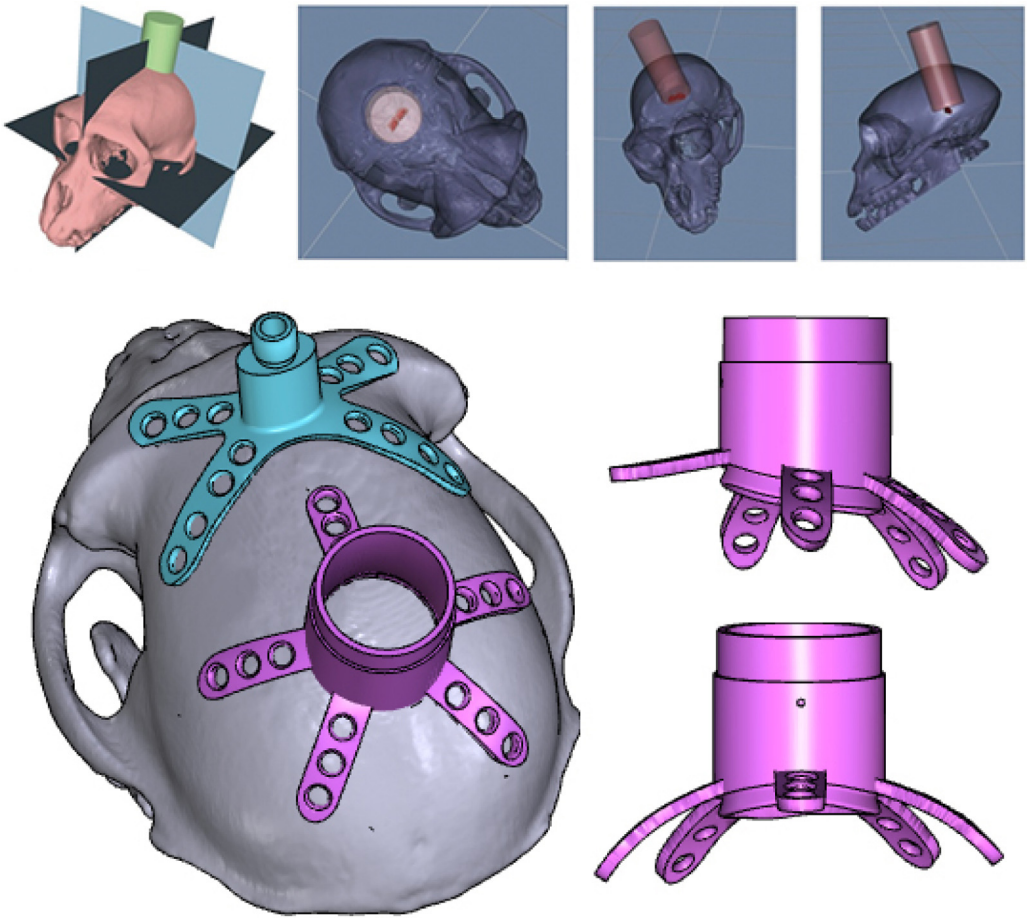

Fig. 8. For superior colliculus recordings, guiding planes were constructed using 3D Slicer software. A cylinder demarcated the volume that would be accessible to depth electrodes, thereby determining the position of our chamber (pink; colours are visible in the online version of the paper).

models were positioned over the skull, close to but not overlapping each other, to minimize the footprint of the base. The customized base and legs of the anchorage base were generated using Blender, and the two pedestals shared a connecting leg. For a more detailed description of how this was carried out, please refer to the documents titled, 'How to model a Cereport baseplate' and 'How to make a wire bundle conduit in a leg' and the template file, 'template_pedestal_anchorage_base.blend' in the Supplementary Information.

2.9. Modelling of craniotomy guides as surgical aids

The implantation of recording chambers and electrode arrays requires careful planning of the craniotomy, which determines the accessibility of brain regions of interest. As part of our pre-surgical planning, we printed surgical guides to aid us during the operation. These animals had previously received a head post implant for head fixation, which we used as landmark. The craniotomy guide consisted of a 'grasper' with a cut-out portion that matched the shape of the head post (allowing the grasper to be fixed to the head post in lock-and-key fashion during surgery), a cutting guide that delineated the boundaries of the craniotomy, and a rod linking the grasper to the cutting guide (Fig. 10). For a more detailed description of how this was carried out, please refer to the document titled, 'How to create a craniotomy guide for chamber implantation' and the template file, 'template_chamber_craniotomy_guide.blend' in the Supplementary Information.

2.10. Visualization of models

All the models were exported in STL format. For easy visualization and sharing, 3D PDF files were generated through a multistep process, which required a combination of software tools. First, each of the models that were associated with an individual animal, such as the skull, the brain, and the implant(s), were imported into MeshLab in STL format, and exported as OBJ files. The OBJ files were then imported into a new project in DAZ Studio 4.7 (Win and Mac, https://www.daz3d.com/daz_studio), and the project was saved as a single U3D file, containing all the models. We downloaded and modified a LaTeX script (Win, Mac and Linux), U3D2PDF (http://www.wiki.david-3d.com/making_a_3d_pdf), and generated an interactive PDF rendering from the U3D file. The 3D PDF file could be shared easily amongst collaborators, and opened in Adobe Acrobat Reader, affording viewers a rotatable and zoomable 3D view of the design. For a more detailed description of how this was carried out, please refer to the document titled, 'How to create a 3D PDF' and the sample LaTeX code, 'sample_3D_PDF_tex_code' in the Supplementary Information.

2.11. 3D printing

We identified 3D printing companies in our region through the online search platform, 3dhubs.com, which allowed us to select printing companies based on the print material, model of the machine, print resolution, geographical location, price, and customer reviews. We consulted various 3D printing companies to ensure that our designs could be printed in precise detail, and

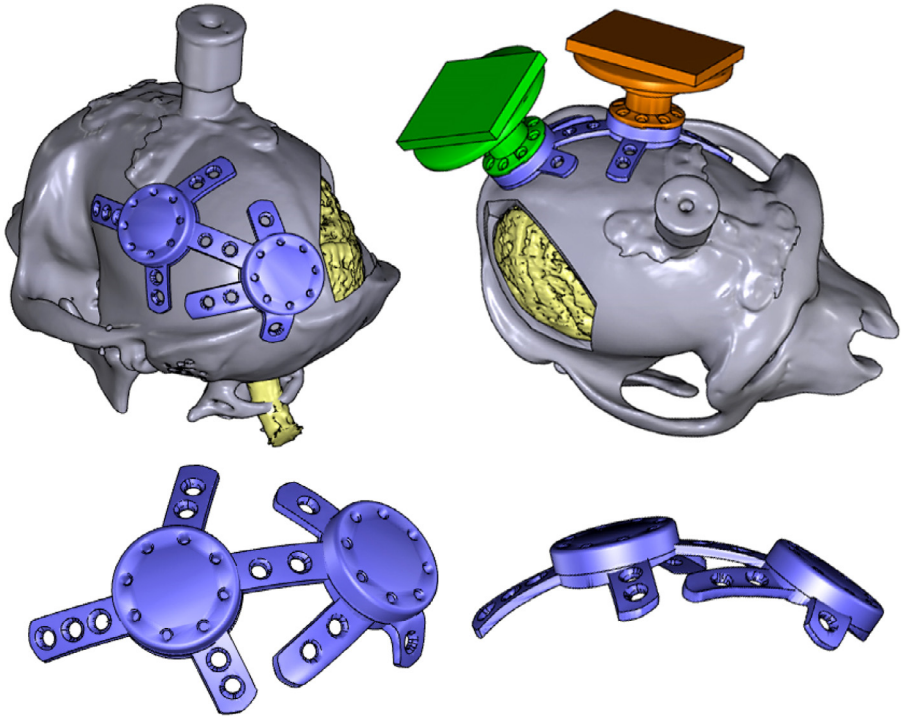

Fig. 9. A virtual craniotomy was made in the skull over the right hemisphere, showing the visual cortex of the brain (yellow; colours are visible in the online version of the paper). A pedestal anchorage base (purple) was created as a support for two CerePort™ pedestals (Blackrock Microsystems, green and orange), and positioned so as to avoid the craniotomy and head post (grey). Note that in this animal, the CT scan of the skull was obtained after the implantation of a (non-customized) head post, hence the skull and head post are fused into one model, and some metal-induced artefacts are visible around the base of the head post.

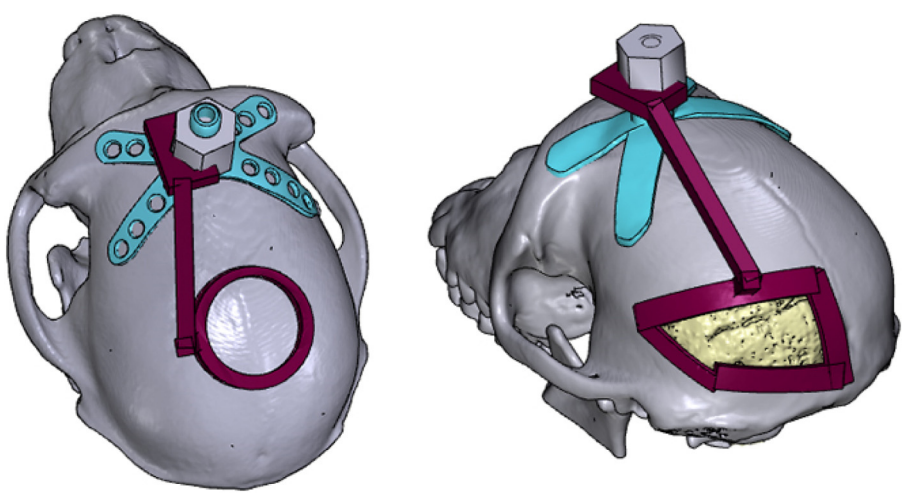

Fig. 10. Craniotomy guides (red) were designed for use during surgical implantation of chambers (left), and electrode arrays (right), allowing the trepanations to be made at the desired locations on the skull (colours are visible in the online version of the paper). Each craniotomy guide consisted of a grasper that could be attached to the head post (blue), and a cutting guide that marked the boundary of the craniotomy.

that their print resolution would be adequate for the task at hand. Table 1 displays the mean cost of each print.

Occasionally, our printers identified minor errors in our models that prevented them from being printed, such as unintended holes and non-manifold edges. We performed mesh repair and clean up using Meshmixer 3.2 software (Win and Mac, http://meshmixer.com). Meshmixer (Autodesk, Inc.) is a popular free software with an 'Inspector' tool that allows the user to analyze a model for errors or irregularities, and fix them rapidly. The software generated solutions to fill small holes and delete unwanted regions – an automated approach that saved us from the substantial time and effort that usually accompanies manual repair.

For cheap and rough rapid prototyping of objects such as the skull, prints were made from acrylnitrile butadiene styrene (ABS) or polylactic acid (PLA) plastic, through a process known as fused deposition modelling (FDM).

For rapid prototyping of objects such as head posts, chambers, pedestal bases and pedestals, we wanted high-quality prints that would closely resemble the final titanium product, with the preservation of fine details. Similarly, our craniotomy guides needed to be accurate in form, but did not have to be made of a strong or expensive implantable material such as metal. For these applications, resin prints were made using stereolithography (SLA), with a Form 1+ 3D printer (Form Labs, Somerville, MA), offering 25-micron

Table 1
Average cost of each type of print, categorized by material, object, and version (P: prototype; F: final object; R: anatomical reference). For rapid prototyping, prints were made from PLA plastic or resin. The craniotomy guides that were used during surgery were printed in clear resin, while the final versions of implants such as the head posts, chambers, and pedestal anchorage base, were printed in Grade 1 titanium. The prices include the cost of post-production that was carried out within the 3D manufacturing company, but do not include post-production that was carried out by our workshop. They also exclude the cost of adding a biocompatible coating to the base (described in section 'Osseo-compatible coating.').

Material	Print	Version	Number of units	Mean cost per unit (€)
Resin	Head post	P	2	21.71
	Pedestal base	P	1	43.14
	Craniotomy guide	F	5	27.68
	Cortex	R	1	36.97
Titanium	Head post	F	7	399.00
	Pedestal base	F	1	355.02
	Chamber	F	2	503.83
PLA plastic	Skull	R	7	36.74

resolution in the vertical dimension. Additionally, prints of segmented cortical tissue were made in resin, and used as anatomical references.

The final implants were printed by an industrial 3D printing company in Grade 1 titanium, using a process known as direct metal printing (DMP). The dimensions of the printed parts had an accuracy of ±50 microns, which was adequate for our purposes.

For a more detailed description of how this was carried out, please refer to the document titled, 'How to 3D print an object' in the Supplementary Information.

2.12. Post-processing

After printing, we carried out further post-production processing. We removed support structures from all the objects. We added external screw threads to the head posts. One of our head posts had a minor defect, causing two of the legs to be bent at an odd angle. We used pliers to bend them into the correct shape.

For the chambers, we added ridges and pins. A disadvantage of 3D printing is that the resolution of the printed objects (~25 μm for resin, ~50 μm for titanium, and ~200 μm for PLA plastic) is typically worse than that which is achievable through CNC machining (~2 μm). As a result, the surface quality of 3D-printed objects is worse than that of CNC-machined objects. We found that this did not affect the overall quality and functionality of our printed objects, except for the interior surface of our chambers, which had to be smoothened in order to facilitate cleaning and reduce the risk of infection. Hence, the interior wall of the chambers was electropolished to a roughness of Ra < 0.05 μm (yielding slight thinning of the material).

For the pedestal anchorage base, we added internal screw threads to the holes on the upper surface. Note that these holes were not oriented perpendicular to the surface, but at an angle of 17.5 degrees, to match the angle of the screw holes on the base of the CerePort™ pedestals. Hence, a special clamp was made to hold the pedestal anchorage base firmly in the correct position and set it at the correct angle during the addition of screw threads (Fig. 11).

Examples of the printed objects are shown in Fig. 12.

2.13. Osseo-compatible coating

Hydroxylapatite (HA) is a synthetic form of calcium phosphate (a naturally occurring component of bones and teeth), which is popularly used as a biomaterial for bone repair and substitution (Surmenev et al., 2014; LeGeros, 2016). Commercial orthopaedic and dental implants are coated with HA granules, to promote

Fig. 11. To add internal screw threads to the holes on the upper surface of the pedestal anchorage base, a special clamp was designed, positioning the holes at a 17.5-degree angle.

osseointegration between the bone and the implant (Søballe et al., 1990; Cook et al., 1992; Lanz et al., 2013; Raphel et al., 2016). The bottom surfaces of our implants were plasma sprayed with HA by the company Medicoat AG (Mägenwil, Switzerland), at a cost of €230 per implant. Note that this procedure is not widely adopted in the field of primate neurobiology, and we have previously observed successful osseointegration of implants that were not coated with HA. Hence, to our knowledge, the benefits of doing so are neither well-researched nor well-established in monkeys. Nevertheless, we felt that the potential benefits merited the additional expenditure. A 30-micron titanium bond layer was added to the lower surfaces of the legs and base, followed by a 50-micron layer of HA. During the coating process, the screw holes were masked to prevent alterations of their dimensions and surface smoothness. For a more detailed description of how this was carried out, please refer to the document titled, 'How to order a coating of hydroxylapatite' in the Supplementary Information.

2.14. Surgical procedure

All experimental surgical procedures complied with the NIH Guide for Care and Use of Laboratory Animals (National Institutes of Health, Bethesda, Maryland), and were approved by the institutional animal care and use committee of the Royal Netherlands Academy of Arts and Sciences.

A course of antibiotics was started two days prior to each operation, and the animal was weighed to obtain the correct dosage. Anaesthesia was induced with intramuscularly administered ketamine (7 mg/kg) and medetomidine (0.08 mg/kg). We administered 0.1 ml atropine (concentration 0.5 mg/ml) if the heart rate dropped below 75 bpm. The animal was placed on a heated mat to allow continuous regulation of body temperature. Eye ointment was applied to maintain hydration of the eyes. Xylocaine ointment was applied to the ear bars of the stereotaxic frame, and the animal's head was secured in the frame.

For maintenance of anaesthesia, the animal was intubated and ventilated with 0.8–1.5% isoflurane (20% O_2 and 80% air). An intravenous catheter was inserted into a vein in the arm. During surgical implantation of head posts and chambers, we administered fentanyl at 0.005 mg/kg on indication, Ringer-glucose at 10–15 ml/kg/hour, and antibiotics intravenously. During surgical implantation of electrode arrays, we additionally administered midazolam at 0.5 mg/kg (concentration 5 mg/ml) once per hour. ECG, heart rate, external blood pressure, SpO_2, CO_2, tempera-

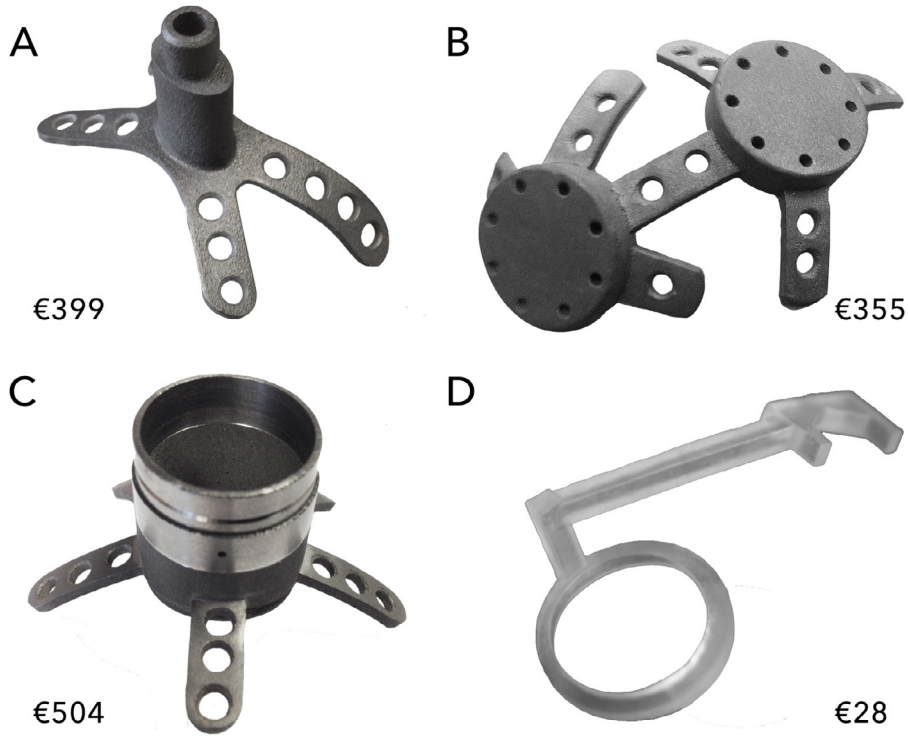

Fig. 12. 3D-printed objects for primate electrophysiology: a head post (A), a pedestal base (B) and a chamber (C) made from titanium, and a craniotomy guide made from resin (D). The price indicated is the average printing cost.

ture, muscle tone, respiration, and the response to pain stimuli were monitored continuously. The head was shaved and cleaned with chlorhexidine solution and alcohol. For installation of cranial implants, a semi-circular flap of skin was carefully detached from the skull over the desired implant location, reflected, and wrapped in damp cotton swabs to keep it moist. Methods of implanting a head post, chamber, and pedestal anchorage base, and post-surgical recovery are described separately in the following sections.

2.14.1. Head post implantation

The titanium head post was autoclaved to ensure sterility. The implant was placed on the skull, with the front legs positioned close to the brow ridge, and adjusted such that it fit perfectly against the skull. We used 2-mm-diameter Ti cortex screws (DePuy Synthes, Amersfoort, Netherlands) to secure the head post to the bone. A small incision was made in the flap of skin, just large enough to allow egress of the head post, and the skin was then pulled over the head post, covering its legs. We positioned the hole in such a way that slight tension was maintained on the skin. The wound margins were sutured together, and an extra stitch was made around the base of the protruding section of the head post, to hold the skin closed around the newly made hole.

2.14.2. Chamber implantation

Prior to use, we sterilized our resin craniotomy guide by soaking it in alcohol for 30 min, and we autoclaved the Ti chamber. For the implantation of chambers (and electrode arrays), in addition to stereotaxic coordinates, we used a craniotomy guide to identify the precise location of the craniotomy, as determined during pre-surgical planning (Fig. 10). First, the guide was affixed to a head post, which had been implanted during an earlier procedure. Next, the circumference of the desired craniotomy was traced using a marker pen, and the craniotomy was made with a trepan. The chamber was positioned over the circular craniotomy and secured to the bone with Ti screws. A small incision was made in the flap of skin, just large enough to allow egress of the chamber. The skin was pulled back over the legs of the chamber and sutured closed. To seal off the chamber, we used a cap from Crist Instrument Co., Inc (Hagerstown, MD), which had an interior rubber ring and was secured using three screws that protruded into a groove running around the outer diameter of the chamber.

2.14.3. Pedestal anchorage base implantation

The titanium pedestal anchorage base was autoclaved to ensure sterility. The implant was adjusted until its position on the skull was correct. Ti screws were used to secure the anchorage base to the bone. We filled the screw holes with bone wax to prevent tissue and fluid egress during the recovery period, in which we expect integration of the implant with the bone. The skin was pulled back over the entire implant and sutured closed. We plan to attach the CerePorts™ during a second surgery in which the arrays will be inserted into the visual cortex.

2.14.4. Recovery

Ten minutes before the end of the surgery, the ventilator was switched to stand-by mode, allowing spontaneous breathing. Upon conclusion of the procedure, the monkey was released from the stereotactical apparatus. The isoflurane was switched off and an antagonist was administered i.m. (atipamezole 0.008 mg/kg), allowing the animal to wake up. Subjects were closely monitored following the operation and given several weeks to recover. For the animal that received a pedestal anchorage plate, a minimum interval of two months is planned between the implantation of the anchorage plate and the implantation of the electrode arrays and CerePorts™. Postoperative care included analgesia with finadyne i.m. (1–2 mg/kg) on the day of the surgery, followed by oral Metacam that was spread on pieces of fruit or mixed with syrup, at 0.1 mg/kg per day, for the six days following the surgery.

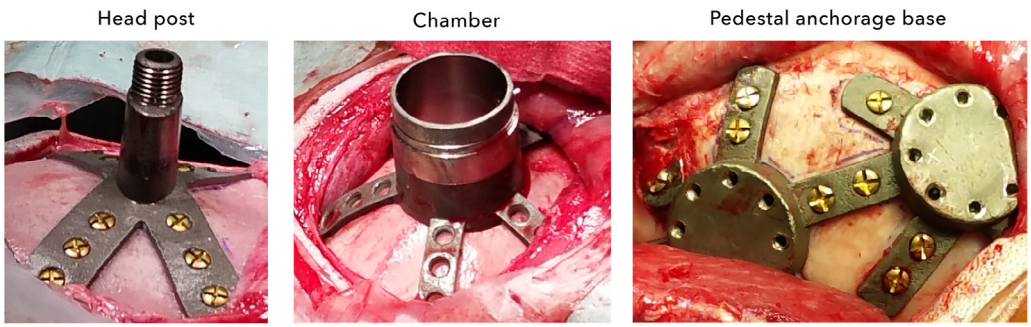

Fig. 13. During surgical implantation, our customized implants sat flush against the surface of the skull, leaving little room for fluid ingress.

3. Results

Compared to non-customized mass-produced implants, our 3D-printed implants were faster and easier to implant, as their base was already optimally or close-to-optimally shaped. For one of our chambers (described in detail below), we had to bend the legs slightly with pliers to obtain a good fit. The other implants needed no further modification during surgery. In all cases, including those where our implants were manually adjusted, we observed little to no gap between the base of the implant and the skull (Fig. 13), reducing the chances of tissue and fluid ingress, and subsequent bacterial infection and tissue inflammation.

At the time of implantation, most of our animals were juveniles, aged 4 to 7 years old, and the time interval between their anatomical scan and the date of implantation was up to 10 months. This raised the question of whether normal cranial development and growth would lead to changes in their bone structure, adversely affecting the fit of the implant. During surgery, however, we observed no effect of elapsed time on the fit of the implant.

3.1. Chamber implantation

In one of the animals that received a chamber, the location indicated by the craniotomy guide perfectly matched that of the stereotaxic coordinates. In the other animal, however, we noticed a discrepancy of approximately 1 cm between the location predicted by the surgical guide and that based on stereotaxic coordinates. We positioned the craniotomy based on the location prescribed by the surgical guide. However, after making the craniotomy and inserting the bottom lip of the chamber into the hole, we found that the chamber legs did not fit perfectly against the bone, making it unlikely that our implantation location was exactly as planned. Hence, we bent the legs with a pair of pliers to match the skull.

In both animals, we found that the craniotomies were slightly too large, hence we filled the gap with dental acrylic. We suspect that this was due to a small mismatch between the size of the hole made by the trepan and the planned size of the chamber. In one animal (the one for which a manual adjustment of the chamber legs was made), the gap was located on only one side of the chamber and measured less than half a millimetre, hence requiring only a small amount of dental acrylic, whereas in the other animal, the gap was larger (although still smaller than 1 mm) and we built up a small layer of dental acrylic around the implant. We plan to make small adjustments to the design of the chambers in future, to prevent the mismatch in size.

3.2. Pedestal anchorage base implantation

To position the pedestal anchorage base on the skull, we did not need to use a surgical guide as this could easily be done by eye. One of the legs of the implant had a distinctive shape that allowed it to fit snugly against the curvature of the occipital ridge (a prominent protrusion of the bone in macaques, as shown in Fig. 6), and we adjusted the position of the implant until a close fit was obtained. We did not observe any gaps between the skull and the implant. Hence, we did not need to modify the legs or use dental acrylic.

Fig. 14. The skin surrounding the customized head post implants showed no signs of retraction in some animals (left), and up to 3 mm of retraction in others. One animal received a pedestal anchorage base (right) and the skin over the implant was healthy, with little sign of the procedure in the months after surgery.

3.3. Implant integration

At the time of writing, the post-surgical implantation period ranged from 11 months to ~2 years and none of our animals developed problems with their customized implants.

In the animals that received customized head posts, we generally observed little retraction of the skin (Fig. 14, left panel), indicating improved health of the surrounding tissue, and good integration between the customized head posts and the skin. This contrasts with our previous experience with non-customized head posts, where we noticed that the skin surrounding the implants sometimes retracted by several millimetres.

For one of the animals that received a customized head post, we carried out a post-operative MRI scan, allowing us to visualize the effects of the metal head post on the quality of the scan. We observed significant artefacts in the region of the brain underlying the head post, extending approximately one centimetre from the base of the head post and occluding the anatomy of the frontal cortex (Fig. 15). However, we were still able to obtain a clear view of the temporal, parietal, and occipital lobes, and visualize the visual cortex (our region of interest in that animal).

At the time of writing, the chambers had been implanted for 13 and 16 months respectively. After surgery, we cleaned the chambers regularly using hydrogen peroxide and betadine solution. The electropolished interior walls were smooth and easy to clean. We did not observe any loss of fluid from the chambers, and they remained stable and free of infection. In one of our animals, the

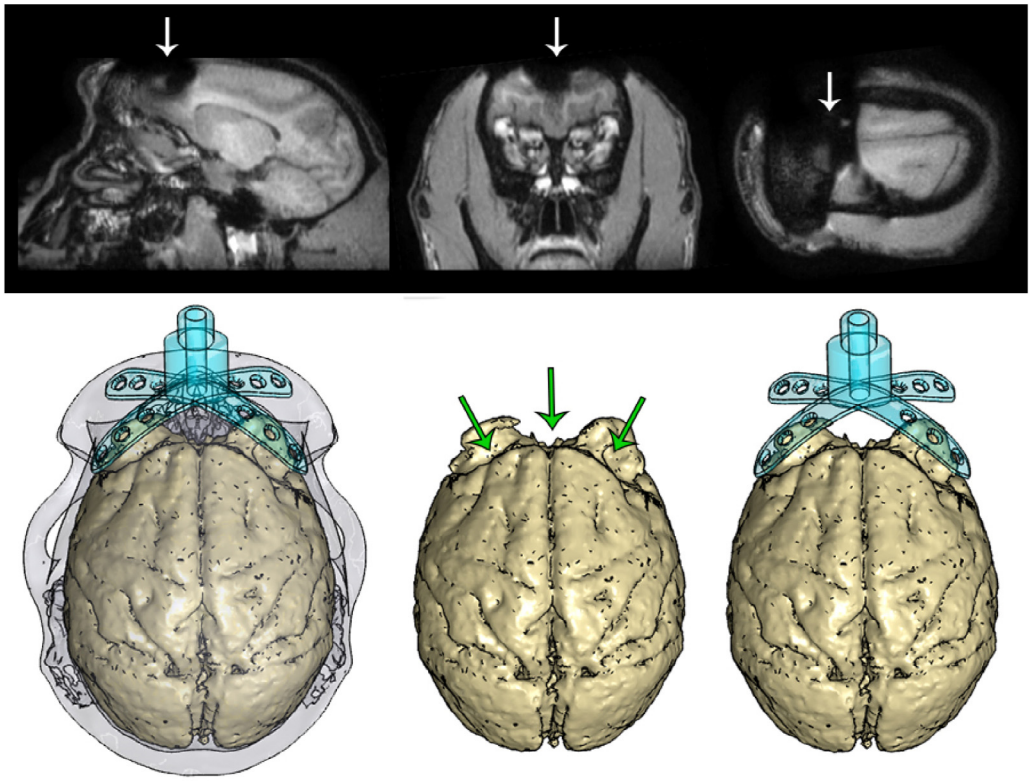

Fig. 15. The titanium head post generated artefacts in a post-operative MRI scan (demarcated by arrows, top), disrupting the signal in the vicinity of the head post and obscuring the anatomy of the frontal lobe. The resulting distortions in the shape of the brain (demarcated by arrows, bottom) closely followed the contours of the legs of the head post.

base and legs of the chamber were not covered with dental acrylic. In this animal, the skin around the chamber remained healthy, with less than 2 mm of retraction around the cylinder base, but retraction occurred over the anterior-most leg of the chamber.

A pedestal anchorage base was implanted in one animal for eight months at the time of writing. The skin was closed back over the implant, allowing the wound to heal fully after the surgery. The overlying skin was healthy with normal fur growth, and the site of implantation was no longer visible a few months after surgery (Fig. 14, right panel), although we were able to feel the raised edges of the anchorage base when palpating the skin.

This same animal had previously been implanted with a non-customized head post. For reasons unrelated to the implantation of the customized pedestal anchorage base, the head post came loose and we carried out a CT scan in order to assess the integrity of the skull underneath the head post. This gave us the opportunity to non-invasively visualize the pedestal anchorage base as well. The metal implant created substantial artefacts in the image, which were identifiable by their bulky forms and jagged surfaces (Fig. 16). We palpated the skin and verified that these structures were indeed artefacts and were not actually present.

4. Discussion

We here described how 3D printing could be used as a powerful tool to speed up surgery time, deliver customized results, and potentially reduce subsequent risk of infection and implant failure. These new techniques were embedded within a larger process, which included more traditional techniques, and substantial planning and post-processing. Setting up a workflow, compiling the requisite software tools, and finding reputable contractors to carry out the printing process required an initial investment of time and energy. Once our protocols were in place, however, this information could be shared readily and used to generate a wide range of well-tailored products. In this Discussion, we cover various aspects of the process, and provide insight into the challenges and advantages of this approach.

4.1. Support and infrastructure

While 3D printing is a highly innovative and even revolutionary technology, representing the forefront of digital design and automated production, the present methods also rely upon an ecosystem of manual labour and machining. Critical to our approach was ready access to MR and CT scanning facilities, along with logistical and technical support, which allowed us to generate 3D models of our animals' anatomy. An alternative strategy is to carry out a surgical survey, in which the skin is temporarily retracted and a mould is taken of the skull, forming the basis for future modelling (Betelak et al., 2001). However, obtaining a cast of the skull is labour-intensive and time-consuming. We also believe that CT or MR scanning is preferable because it avoids an additional surgical procedure. McAndrew et al. (2012) have previously attempted to perform a non-invasive 'skull mapping' procedure in an awake animal, using a stereotaxic needle to scan the head in three dimensions (with the skin intact) in order to generate a 3D representation of the skull. However, this failed to accurately capture the morphology of the skull (perhaps due to the overlying muscle and skin tissue), and the authors abandoned this approach for MRI and CT data acquisition.

Throughout the design process, we worked closely with our mechanical workshop and 3D printing service providers, obtaining advice on the design considerations to be taken with our prints. Some of these arose from the constraints imposed by 3D printing technology, while others were related to principles in engineering, such as the calculation of tolerances, dimensions of screw holes and

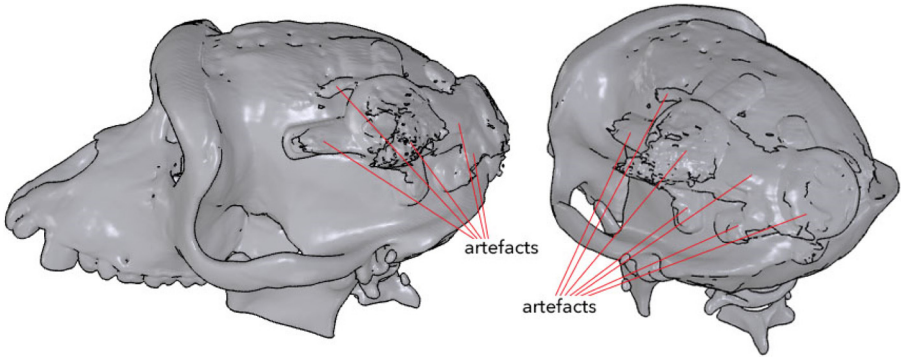

Fig. 16. A CT scan revealed the overall contours of the pedestal anchorage base, although numerous artefacts were generated in the image, due to the metallic nature of the implant.

screw threads, and material strength. If we anticipated that certain tools might be needed during the post-processing stage, such as thread cutters or clamps with which to securely hold our prints, these were ordered or made in advance by our workshop.

With a choice of numerous rapid prototyping companies in our region, we had our plastic and resin prints made by several service providers, and selected the providers who offered the best value. On occasion, prints were ready for collection as soon as the day after placement of the order. The prompt service and good print quality allowed the production process to proceed rapidly.

For our titanium prints, we benefitted from geographical proximity to both a leading industrial 3D printing company, and a medical coating company (MediCoat, Switzerland). Due to their short production times, we typically received our new titanium prints within three weeks from the date that the order was placed, while coating of prints with HA took one to two weeks from the date that the medical coating company received the implant.

After the titanium parts were printed, post-processing work included electro-polishing of the interiors of chambers, which was carried out by a third-party company. Our mechanical workshop added ridges and pins to chambers, and screw threads to head posts and the pedestal anchorage base. Two of our head posts had slight defects due to printing and/or design errors; however, we were able to rectify them easily by bending the legs with pliers.

4.2. 3D printing materials

The machines on which our prints were built ranged from desktop printers, such as the Ultimaker and the Form, to industrial printers that printed in metal. Whenever possible, we printed high-quality prototypes to check and evaluate our designs, before printing them at higher cost in titanium. The relatively low cost of the prototype prints allowed us to take advantage of the benefits offered by 3D printing: the ability to quickly create unique, complex implants that were customized to individual animals, and freedom from the design constraints imposed by traditional CNC milling methods.

To ensure that our designs would be printable, we acquired a basic understanding of how various 3D printers work. FDM printers (for plastic prints) build their objects in the air, layer by layer, while SLA printers (for resin prints) build their objects from a solution. During the printing process, both FDM and SLA printers add extra material known as 'support structures' to the print. The support structures act as scaffolds and prevent the print from deforming due to gravity. Many commonly used FDM printers, such as the Ultimaker, are hobbyist machines, which tend to produce their prints relatively quickly and at low resolution. They build prints out of plastics that have low melting temperatures, and can often yield uneven results. Due to the properties of the print material and the deposition process, FDM prints can be fragile, especially at thin points. Similarly, when it comes to printing using SLA, low-cost resin prints tend to become brittle when exposed to UV light and may therefore fall apart over time. Hence, unless these low-cost plastic or resin prototypes are intended for short-term use, their form should be robust in design. We do note, however, that the range of materials on offer continues to expand. For higher prices, it is possible to produce prototypes using materials that confer properties such as additional strength, toughness, biocompatibility, and flexibility to the prints.

Unlike plastic and resin prints, titanium prints are built up layer by layer within a bed of metal titanium particles. Hence, they do not require additional structures to support their weight. The titanium particles are fused together at high temperatures by a laser beam, yielding extremely strong, durable prints, which accounts for the popularity of this technique in the aerospace, automotive, and health industries. Medical implants are typically manufactured using medical-grade titanium, and various methods of enhancing their biocompatibility are under development. These include the coating of implants with osteocompatible materials such as calcium phosphates, the embedding of bactericidal silver particles into the osteocompatible coating (Valle et al., 2012; Lanz et al., 2013), and the creation of nano-scale pores on the surface of the implants via metal laser sintering, grit blasting, or acid etching, in order to promote osseointegration (Buser et al., 1991; Hacking et al., 2012; Raphel et al., 2016). Titanium has the added advantage of being ductile enough to be bent manually with pliers, if the need arises (e.g. during surgical implantation of one of our chambers, we performed manual bending of the legs, due to a discrepancy between the planned and actual location of the implant).

We note that if an animal with a metal implant undergoes a structural MR or CT scan, the implant is likely to distort the magnetic field and produce artefacts in the signal, which may obscure the anatomy of the brain and/or skull in the region of the implant (as seen in Figs. 15 and 16). Hence, any anatomical or functional scans of the brain should ideally be obtained prior to implantation with a titanium object, particularly if the location of the implant is close to that of the brain region of interest. Nevertheless, under certain circumstances, it may be useful to carry out an anatomical scan – such as when the researchers want to verify the location of an inserted electrode, or check the quality of the underlying bone and assess the level of integration between the skull and the implant (Adams et al., 2007). We would refrain from performing functional scans in animals with a metallic head post, due to concern over potential overheating of the implant, and also because this is not widely done (further research on the thermal conductance properties of various metals in an MR scanner might be useful). Radiolucent materials,

such as PEEK, are widely used in applications that require extensive post-operative scanning (Mulliken et al., 2015), in combination with ceramic (rather than titanium) screws. However, 3D printing in PEEK is still at a relatively early stage of development, hence radiolucent implants are usually manufactured through CNC milling (McAndrew et al., 2012; Lanz et al., 2013).

Besides plastics, resins and metals, biologically inspired materials are starting to be developed. Recently, a study demonstrated the use of a novel synthetic osteoregenerative material, termed 'hyperelastic bone,' which is composed of hydroxylapatite (90%) and polycaprolactone or poly(lactic-co-glycolic-acid) (10%) (Jakus et al., 2016). This material could be rapidly 3D printed, and had properties mimicking that of naturally occurring bone, such as high porosity, elasticity and strength. A cranial implant made out of hyperelastic bone was used to repair a defect in the skull of a monkey (Jakus et al., 2016), and the researchers found that it integrated readily with the bone and was well vascularized just four weeks after the surgery, making it a promising material for the creation of future implants in neuroscience.

4.3. 3D modelling software

We explored a wide variety of 3D modelling tools, with a focus on free, open-source software. InVesalius, OsiriX, FSL, and 3D Slicer were used for processing CT and MR imaging data, while Blender, MeshLab, and DAZ Studio were used for 3D design and rendering. Imaging data is typically stored in the DICOM format, and is readily accessible through a number of software tools. However, a plethora of file formats are used in 3D modelling- the most popular of which include the STereoLithography (STL), OBJect (OBJ), and PoLYgon (PLY) formats. Each programme was able to handle a specific set of 3D file formats, necessitating a diverse range of software to cover all the functions required. We hope that other researchers will be able to take advantage of the proposed workflow (Table 2), thereby reducing the time needed to identify the necessary software tools and their interfaces so that they can quickly assemble their own coherent workflow. We have also assembled a series of reference manuals that are available for download in the Supplementary Information (please refer to Section 4.6, 'Sharing amongst researchers').

4.4. Craniotomies

In one of our SC animals, our craniotomy guides were combined successfully with pre-surgical planning and stereotaxic measurements, providing us with accurate delineations of the craniotomy boundaries. Furthermore, the precisely tailored fit of our implant helped to verify that it was correctly positioned on the skull during implantation, as slight deviations from the planned location yielded a suboptimal fit. In some cases, such customization can reduce or eliminate the need for researchers to undertake post hoc imaging studies to determine the optimal trajectory of electrodes that are inserted through a chamber (Kalwani et al., 2009). For example, we successfully obtained recordings from the superior colliculus in one of our animals via a customized recording chamber, without needing to carry out a post-operative scan (at the time of writing, we have not started recording from the other animal, but we also expect that a scan will not be necessary). Nevertheless, these methods are not always foolproof. In one animal, we noticed a disparity between the surgical guide and the intended stereotactic coordinates, as well as an imperfect fit between the chamber and the skull. We expect the likelihood of these mismatches to decrease as researchers gain experience with these methods.

In both animals, we found that the craniotomy was slightly too large relative to the diameter of the chamber and we used dental acrylic to fill in the gaps. Hence, the exact size of the printed chamber should be carefully measured and compared to the trepan to ensure as close a fit as possible. As an alternative to dental acrylic, one could consider using Geristore® (DenMat, Lompoc, CA), a resin ionomer which reportedly offers several advantages over dental acrylic such as enhanced biocompatibility (Johnston et al., 2016), or a hydroxylapatite paste such as Mimix QS (Biomet Microfixation, Jacksonville, FL) (Adams et al., 2011).

4.5. Design considerations

During the 3D modelling process, we considered several designs for our implants. For example, we tested various configurations for the layout of our pedestal anchorage base, and adjusted the number of legs and their positions. During surgery, we found that one of the legs of the anchorage base extended laterally under the muscle tissue surrounding the implantation site, slightly impeding access to one of the screw holes. Hence, for future implants, we plan to generate a 3D model of the overlying skin and muscle tissue from our MRI scans, to ensure that the legs and screw holes are readily accessible.

All of our designs featured multiple legs per implant. A disadvantage of this is that the raised profile of the legs may cause the skin to recede from the implant, eventually exposing the bone (Mulliken et al., 2015). This only occurred in one of our implants (a chamber), for just one of its legs. The problematic leg was positioned close to an existing head post, which may have contributed to the retraction of the skin. An alternative technique, described by Mulliken et al. (2015) for the creation of customized PEEK chambers, is to embed the screw holes within the wall of the chamber itself (Mulliken et al., 2015). Downsides to this approach are that the circumference of the chamber is increased, and the anchor points of the screws are concentrated within a small region rather than distributed over a larger area, which may contribute to mechanical instability.

Adams et al. (2007) have reported using titanium head posts with feet of a similar thickness to ours (1 mm), and they found that 14 months after implantation, the bone had grown over the feet, partially embedding the head posts and screws within the skull. We generally observed little retraction of the percutaneous wound margin in our animals, perhaps due to the precautions taken during surgery to keep the skin firmly wrapped around our implants, as well as to the low profile of our feet (~1 mm).

We identified several improvements that could be made to the design of our chambers. Firstly, we electropolished the interior of our chambers, as well as the upper half of the exterior. In one animal, we found that the lower half of the chamber exterior tended to accumulate dirt due to its rough surface. Hence, we plan to electropolish the whole cylinder in future iterations (though not the legs). Secondly, the design of our chambers included a pin that protruded from the exterior wall of the chamber; however, during recordings from the SC, we found that the pin was unnecessary and limited the number of positions that could be accessed using our microdrive, and we may choose to eliminate the pin from subsequent designs. Thirdly, our chambers were designed with a lower 'lip' around the base of the cylinder, which extended below the surface of the skull, and enhanced the seal between the chamber and the bone. However, the presence of the lip prevented us from testing the fit of the chamber legs against the skull, prior to making the craniotomy. Hence, for future chamber implantations, we plan to print out a lipless version of the chamber in resin, which will be used to determine the exact position of the chamber, based on the fit between the skull and the chamber legs, before carrying out the craniotomy. We could even combine the lipless resin chamber with our craniotomy guide, producing a single chamber-craniotomy resin guide.

Table 2
Workflow for each type of printed object, listing the software and file formats that were involved. The numbers in the 'Output' columns refer to the order of the steps involved. '1/2' indicates that these steps could be performed simultaneously or in any order.

Steps	Description	Software	File formats	Output					
				Skull model	Brain model	Head post	Chamber	Pedestal base	Craniotomy guide
CT scan	Obtain anatomical scans of skull	–	DICOM	1		1	1/2	1/2	1/2
MRI scan	Obtain anatomical scans of brain and/or blood vessels	–	DICOM		1		1/2	1/2	1/2
3D modelling of skull	Generate model of skull, identify anatomical landmarks	InVesalius/OsiriX, MeshLab	STL	2	2	2	3	3	3
3D modelling of brain	Generate model of brain, identify anatomical landmarks	3D Slicer/FSL, MeshLab	STL				4	4	4
3D modelling of object	Align anatomical models, design customized objects	3D Slicer, Blender/Inventor	STL			3	5	5	5
Generate STL/PDF files	Generate STL files for printing and 3D PDF files for sharing	MeshLab, DAZ Studio, LaTeX	STL, OBJ, U3D, PDF	3	3	4	6	6	6
3D print in plastic	Create rapid prototypes using fused deposition modelling	Meshmixer[a]	STL	4					
3D print in resin	Create high-resolution resin prints using stereolithography	Meshmixer[a]	STL		4	5	7	7	7
3D print in Ti	Create titanium implants using direct metal printing	Meshmixer[a]	STL			6	8	8	
Machining	Post-production processing and correction of defects	–	–			7	9	9	
Coating with HA	Coat base of implants with layer of hydroxylapatite	–	–			8	10	10	
Sterilization	Soak resin prints in alcohol, and autoclave titanium prints	–	–			9	11	11	8

[a] MeshMixer was used only if minor repairs were needed prior to printing.

4.6. Sharing amongst researchers

Once our workflow was established, we were able to share these techniques easily between lab members. While the base and legs of our implants were customized to the anatomy of individual animals, design elements such as the tops of chambers and head posts were standardized between animals, to allow mating with the microdrives and head post holders used in our lab. We generated a series of manuals, along with Blender template files for our 3D models that contained 'building blocks' for each type of implant. These manuals and template files are available for download as supplementary information. The use of open-source software facilitated file sharing and skill and knowledge transfer, allowing researchers to become proficient in the entire 3D modelling and printing process within weeks. If essential infrastructure such as a mechanical workshop, scanning facility, and 3D printing services are available, it is likely that this system can be readily implemented in other labs.

4.7. Cost

Several large companies offer 3D metal printing services 'on-demand,' providing access to leading-edge industrial 3D printers that produce high-quality metal parts. Typically, the cost price of such printers starts at several hundred thousand euros, going up to €1 M or more, depending on the model. Due to the low setup costs for each print, such companies are able to produce customized, one-off solutions that cater specifically to the medical, dental, and research markets.

The commercially produced customized implants that are offered by neuroscience research companies tend to be built using CNC milling techniques, rather than 3D printing. The cost price of such implants includes labour and overhead costs, as well as the cost of equipment and materials, and the company's profit margin. Hence, it is not entirely straightforward to compare the overall costs of implant production between commercially offered products and the 3D-printed solutions developed by our lab. To our knowledge, however, our customized implants are substantially cheaper, particularly when it comes to recording chambers. For customized head posts, the most competitive commercially available solutions of which we are aware are slightly more expensive than our titanium head posts (€399 on average for the materials), even when labour costs are factored in for the design of the customized implants. Therefore, cost considerations alone should not deter researchers from using 3D-printed implants.

4.8. Implications for research

Poorly designed implants that do not conform to the unique curvature of an animal's skull can result in higher risk of infection, tissue growth, and eventually, implant failure. Loss or breakage of an implant requires an emergency repair surgery (Adams et al., 2007), and if possible, re-implantation, causing additional physical and emotional stress for the animal, and often disrupting experimental data collection. An increase in the quality of implants leads to better stability and longevity of neuronal recordings, improved wellbeing of the animals, and better scientific results. Due to the small numbers of animals involved in our studies, and the presence of other potentially confounding factors (such as the overall health of each animal, or the level of maintenance of the wound margins by individual researchers), our results are primarily qualitative, and our observations are based on visual examinations made by the lab researchers, animal technicians, and veterinarians. Nevertheless, we note that none of our customized implants have given rise to problems with infection or loosening from the cranium thus far, and the retraction of the skin around the implants appears to be less than that typically observed with non-customized implants. The field of 3D printing has expanded and matured, making its techniques accessible to research labs, at prices that rival those of off-the-shelf products, thus offering a strong incentive for scientists to use customized 3D-printed implants for their research.

Funding

This work was supported by the NWO (ALW grant number 823-02-010) and the European Union (the Human Brain Project and ERC Grant Agreement number 339490 "Cortic_al_gorithms").

Acknowledgements

We thank Kor Brandsma and Anneke Ditewig for technical support, Matthew Self, Eric Avila, Geert Springeling, and Rob Teeuwen for assistance during the design of the implants, Ruud van der Blom, Joost Brand and Stephen Super for help with mechanical engineering, and Cyril Voisard (Medicoat) and Rob Franklin and Kian Torab (Blackrock Microsystems) for assistance during several of the processing steps.

Appendix A. Supplementary data

Supplementary data associated with this article can be found in the online version, at http://dx.doi.org/10.1016/j.jneumeth.2017.05.013. The supplementary information consists of manuals and template files to guide the reader through the process of creating anatomical models, customized cranial implants, and surgical guides. Please refer to the 'readme' file in the supplementary information for further information.

References

Adams, D.L., Economides, J.R., Jocson, C.M., Horton, J.C., 2007. A biocompatible titanium headpost for stabilizing behaving monkeys. J. Neurophysiol. 98 (2), 993–1001.

Adams, D.L., Economides, J.R., Jocson, C.M., Parker, J.M., Horton, J.C., 2011. A watertight acrylic-free titanium recording chamber for electrophysiology in behaving monkeys. J. Neurophysiol. 106 (3), 1581–1590.

Avila, E., Godschalk, M., Springeling, G., Roelfsema, P.R., Frens, M.A., de Zeeuw, C.I., 2012. Personalized recording chamber design and neurophysiological planning for non-human primates using an MRI. In: C7/Cerebnet Consortium Joint Meeting. Amsterdam., pp. 1-1.

Baden, T., Chagas, A.M., Gage, G., Marzullo, T., Prieto-Godino, L.L., Euler, T., 2015. Open Labware: 3-D printing your own lab equipment. PLoS Biol. 13 (3), e1002086–e1002112.

Betelak, K.F., Margiotti, E.A., Wohlford, M.E., Suzuki, D.A., 2001. The use of titanium implants and prosthodontic techniques in the preparation of non-human primates for long-term neuronal recording studies. J. Neurosci. Methods 112, 9–20.

Buser, D., Schenk, R.K., Steinemann, S., Fiorellini, J.P., Fox, C.H., Stich, H., 1991. Influence of surface characteristics on bone integration of titanium implants. A histomorphometric study in miniature pigs. J. Biomed. Mater. Res. 25 (7), 889–902.

Campbell, P.K., Jones, K.E., Huber, R.J., Horch, K.W., Normann, R.A., 1991. A silicon-based, three-dimensional neural interface: manufacturing processes for an intracortical electrode array. IEEE Trans. Biomed. Eng. 38 (8), 758–768.

Chae, M.P., Rozen, W.M., McMenamin, P.G., Findlay, M.W., Spychal, R.T., Hunter-Smith, D.J., 2015. Emerging applications of bedside 3D printing in plastic surgery. Front. Surg. 2, 1–14.

Chia, H.N., 2015. Recent advances in 3D printing of biomaterials. J. Biol. Eng. 9 (4), 1–14.

Collinger, J.L., Wodlinger, B., Downey, J.E., Wang, W., Tyler-Kabara, E.C., Weber, D.J., et al., 2013. High-performance neuroprosthetic control by an individual with tetraplegia. The Lancet 381 (9866), 557–564.

Cook, S.D., Thomas, K.A., Dalton, J.E., Volkman, T.K., Whitecloud III, T.S., Kay, J.F., 1992. Hydroxylapatite coating of porous implants improves bone ingrowth and interface attachment strength. J. Biomed. Mater. Res. 26, 989–1001.

Evarts, E.V., 1966. Methods for recording activity of individual neurons in moving animals. In: Potter, V., Rushmer, R. (Eds.), Methods in Medical Research. Year Book Medical Publishers, Chicago, IL, pp. 241–250.

Flesher, S.N., Collinger, J.L., Foldes, S.T., Weiss, J.M., Downey, J.E., Tyler-Kabara, E.C., et al., 2016. Intracortical microstimulation of human somatosensory cortex. Sci. Transl. Med. 8, 1–10.

Galashan, F.O., Rempel, H.C., Meyer, A., Gruber-Dujardin, E., Kreiter, A.K., Wegener, D., 2011. A new type of recording chamber with an easy-to-exchange microdrive array for chronic recordings in macaque monkeys. J. Neurophysiol. 105 (6), 3092–3105.
Gardiner, T.W., Toth, L.A., 1999. Stereotactic surgery and long-term maintenance of cranial implants in research animals. Contemp. Top. Lab. Anim. Sci. 38 (1), 56–63.
Hacking, S.A., Boyraz, P., Powers, B.M., Sen-Gupta, E., Kucharski, W., Brown, C.A., et al., 2012. Surface roughness enhances the osseointegration of titanium headposts in non-human primates. J. Neurosci. Methods 211 (2), 237–244.
Isoda, M., Tsutsui, K.-I., Katsuyama, N., Naganuma, T., Saito, N., Furusawa, Y., et al., 2005. Design of a head fixation device for experiments in behaving monkeys. J. Neurosci. Methods 141 (2), 277–282.
Jakus, A.E., Rutz, A.L., Jordan, S.W., Kannan, A., Mitchell, S.M., Yun, C., et al., 2016 Sep 28. Hyperelastic "bone": A highly versatile, growth factor-free, osteoregenerative, scalable, and surgically friendly biomaterial. Sci. Transl. Med. 8 (358), 1–16.
Johnston, J.M., Cohen, Y.E., Shirley, H., Tsunada, J., Bennur, S., Christison-Lagay, K., et al., 2016. Recent refinements to cranial implants for rhesus macaques (*Macaca mulatta*). Lab. Anim. 45 (5), 180–186.
Kalwani, R.M., Bloy, L., Elliott, M.A., Gold, J.I., 2009. A method for localizing microelectrode trajectories in the macaque brain using MRI. J. Neurosci. Methods 176 (2), 104–111.
Lanz, F., Lanz, X., Scherly, A., Moret, V., Gaillard, A., Gruner, P., et al., 2013. Refined methodology for implantation of a head fixation device and chronic recording chambers in non-human primates. J. Neurosci. Methods 219 (2), 262–270.
LeGeros, R.Z., 2016. Properties of osteoconductive biomaterials: calcium phosphates. Clin. Orthop. 395, 81–98.
Li, X., Morgan, P.S., Ashburner, J., Smith, J., Rorden, C., 2016. The first step for neuroimaging data analysis: DICOM to NIfTI conversion. J. Neurosci. Methods 264, 47–56.
McAndrew, R.M., VanGilder, J.L.L., Naufel, S.N., Tillery, S.I.H., 2012. Individualized recording chambers for non-human primate neurophysiology. J. Neurosci. Methods 207 (1), 86–90.
McDougal, R.A., Shepherd, G.M., 2015. 3D-printer visualization of neuron models. Front. Neuroinf. 9, 1–9.
Mok, S.-W., Nizak, R., Fu, S.-C., Ho K-WK, Qin, L., Saris, D.B.F., et al., 2016. From the printer: Potential of three-dimensional printing for orthopaedic applications. J. Orthopaedic Transl. 6 (C), 42–49.
Mulliken, G.H., Bichot, N.P., Ghadooshahy, A., Sharma, J., Kornblith, S., Philcock, M., et al., 2015. Custom-fit radiolucent cranial implants for neurophysiological recording and stimulation. J. Neurosci. Methods 241, 146–154.
Murphy, S.V., Atala, A., 2014. 3D bioprinting of tissues and organs. Nat. Biotechnol. 32 (8), 773–785.
Nicolelis, M.A.L., Dimitrov, D., Carmena, J.A., Crist, R., Kralik, J.D., Wise, S.P., 2003. Chronic, multisite, multielectrode recordings in macaque monkeys. PNAS 100 (19), 11041–11046.
Nordhausen, C.T., Rousche, P.J., Normann, R.A., 1994. Optimizing recording capabilities of the Utah Intracortical Electrode Array. Brain Res. 637, 27–36.
Parthasarathy, J., 2014. 3D modeling, custom implants and its future perspectives in craniofacial surgery. Ann. Maxillofac. Surg. 4 (1), 9–10.
Patel, S.R., Ghose, K., Eskandar, E.N., 2014. An open source 3-D printed modular micro-drive system for acute neurophysiology. Ginsberg SD, editor. PLoS ONE 9 (4), e94262–e94310.
Paxinos, G., Huang, X.-F., Toga, A.W., 1999. The Rhesus Monkey Brain in Stereotaxic Coordinates. Academic Press.
Pigarev, I.N., Nothdurft, H.-C., Kastner, S., 1997. A reversible system for chronic recordings in macaque monkeys. J. Neurosci. Methods 77, 157–162.
Raphel, J., Holodniy, M., Goodman, S.B., Heilshorn, S.C., 2016. Multifunctional coatings to simultaneously promote osseointegration and prevent infection of orthopaedic implants. Biomaterials 84 (C), 301–314.
Rengier, F., Mehndiratta, A., Tengg-Kobligk von, H., Zechmann, C.M., Unterhinninghofen, R., Kauczor, H.U., et al., 2010. 3D printing based on imaging data: review of medical applications. Int. J. CARS 5 (4), 335–341.
Rose, A.S., Kimbell, J.S., Webster, C.E., Harrysson, O.L.A., Formeister, E.J., Buchman, C.A., 2015a. Multi-material 3D models for temporal bone surgical simulation. Annals of Otology, Rhinology and Laryngology 124 (7), 528–536.
Rose, A.S., Webster, C.E., Harrysson, O.L.A., Formeister, E.J., Rawal, R.B., Iseli, C.E., 2015b. Pre-operative simulation of pediatric mastoid surgery with 3D-printed temporal bone models. Int. J. Pediatr. Otorhinolaryngol. 79 (5), 740–744.
Surmenev, R.A., Surmeneva, M.A., Ivanova, A.A., 2014. Significance of calcium phosphate coatings for the enhancement of new bone osteogenesis – a review. Acta Biomater. 10 (2), 557–579.
Søballe, K., Hansen, E.S., Brockstedt-Rasmussen, H., Pedersen, C.M., Bünger, C., 1990. Hydroxyapatite coating enhances fixation of porous coated implants. Acta Orthop. Scand. 61 (4), 299–306.
Tek, P., Chiganos, T.C., Mohammed, J.S., Eddington, D.T., Fall, C.P., Ifft, P., et al., 2008. Rapid prototyping for neuroscience and neural engineering. J. Neurosci. Methods 172 (2), 263–269.
Valle, Della C., Visai, L., Santin, M., Cigada, A., Candiani, G., Pezzoli, D., et al., 2012. A novel antibacterial modification treatment of titanium capable to improve osseointegration. IJAO 35, 1–12.
Weber, B., Keller, A.L., Reichold, J., Logothetis, N.K., 2008 Sep 15. The microvascular system of the striate and extrastriate visual cortex of the macaque. Cereb. Cortex 18 (10), 2318–2330.
Wu, G.-H., Hsu, S.-H., 2015. Review: polymeric-based 3D printing for tissue engineering. J. Med. Biol. Eng. 35 (3), 285–292.